Applied Physics Letters

Laser-induced morphology-switchable slanted shape memory microcones for maneuvering liquid droplets and dry adhesion

Cite as: Appl. Phys. Lett. **120**, 061603 (2022); https://doi.org/10.1063/5.0077521
Submitted: 03 November 2021 • Accepted: 28 January 2022 • Published Online: 08 February 2022

Chuanzong Li, Yunlong Jiao, Dayu Li, et al.

AIP Publishing

Applied Physics Letters ARTICLE scitation.org/journal/apl

Laser-induced morphology-switchable slanted shape memory microcones for maneuvering liquid droplets and dry adhesion

Cite as: Appl. Phys. Lett. **120**, 061603 (2022); doi: 10.1063/5.0077521
Submitted: 3 November 2021 · Accepted: 28 January 2022 ·
Published Online: 8 February 2022

Chuanzong Li,[1] Yunlong Jiao,[2] Dayu Li,[1] Longfu Li,[3,4] Yubin Peng,[5] Shaojun Jiang,[5] Yiyuan Zhang,[5] Cong Zhang,[5] Shengying Fan,[5] Qingrui Song,[2] Jianquan Li,[1,6] Yi Xiao,[7] Sizhu Wu,[1,6,a)] and Chao Chen[8,a)]

AFFILIATIONS

[1]School of Instrument Science and Opto-Electronics Engineering, Hefei University of Technology, Hefei 230009, China
[2]Institute of Tribology, Hefei University of Technology, Hefei 230009, China
[3]Key Laboratory of Optoelectronic Devices and Systems of Ministry of Education/Guangdong Province, College of Physics and Optoelectronic Engineering, Shenzhen University, Shenzhen 518060, China
[4]Shenzhen Key Laboratory of Photonic Devices and Sensing Systems for Internet of Things, Guangdong and Hong Kong Joint Research Centre for Optical Fibre Sensors, Shenzhen University, Shenzhen 518060, China
[5]CAS Key Laboratory of Mechanical Behavior and Design of Materials, Department of Precision Machinery and Precision Instrumentation, University of Science and Technology of China, Hefei 230026, China
[6]Anhui Province Key Laboratory of Measuring Theory and Precision Instrument, Hefei University of Technology, Hefei 230009, Anhui, China
[7]School of Mechanical Engineering, Nantong Vocational University, Nantong 226007, China
[8]College of Materials Science and Engineering, Hefei University of Technology, Hefei 230009, China

[a)]**Authors to whom correspondence should be addressed:** sizhuwu@hfut.edu.cn and chaoc11@ustc.edu.cn

ABSTRACT

Slanted micro-/nano-structures play pivotal roles in a diversity of fields, including water-proof engineering and fogdrop collection. In light of recent advances in fabricating slanted microstructures by using photolithography or reactive ion etching techniques, however, a complex, environmentally unfavorable, and tedious fabrication process makes them far from practical in application. Herein, we present a viable strategy to prepare a slanted shape memory microcone array (SSMMA) by combining the femtosecond laser oblique microfabrication and replica-mold method. Thanks to its fast temperature-responsive feature, SSMMA enables the transition of adhesion forces to effectively control the sliding of droplet on the surface. The underlying principle of the adjustable migration behavior of droplet is that SSMMA switches between the slanted and collapsed states. Moreover, we systematically studied the influence of the microcone spacing/height together with the microcone bending angle on the wetting performance of water droplet. More significantly, the resulted SSMMA analogous to a "machine hand" is experimentally demonstrated to be competent for the grab and transfer of fragile and smooth objects (e.g., coverslip) with a maximum adhesion force of ∼19.404 mN. The current study opens up an avenue for rapidly fabricating functional slanted microstructures for practical usage.

Nature, as a precious source, provides a wealth of inspiration for designing and fabricating structures with exceptional characteristics.[1,2] The directed microstructure of the butterfly's wing allows it to prevent the adherence of water droplets.[3] Water striders can move fast on the water surface due to the vast number of oriented tiny hairs on their legs,[4] implying that the oriented microstructures play a significant role in biological communities. Therein, slanted microstructures have attracted extensive interest owing to their unique characteristics. For example, the awned wheat[5–7] and cacti[8–10] can survive in arid areas depending on their slender sloping awns and oriented conical spines, which enables them a capability of capturing droplets in foggy environments. These interesting phenomena provide great insights to

design biomimetic surfaces for liquid manipulation and adhesion maneuvering. In this consideration, harvesting a slanted topography is regarded as a prerequisite for realizing intentional functionalities, such as droplet manipulation and dry adhesion.

To obtain a biomimetic slanted microstructure, several impressive fabricating methods have been proposed. For instance, by combining the projection lithography and deep reactive ion etching (DRIE) and gold film deposition techniques, Chu *et al.*[11] obtained the slanted micropillar arrays with different bending angles for unidirectional liquid spreading. Malvadkar *et al.*[12] prepared tilted poly(p-xylylene) nanorod arrays with unidirectional wetting properties by bottom–up vapor-phase oblique angle polymerization (VPP) technique. Wang[13] and Jeong *et al.*[14] prepared the slant micropillars/nanohairs by an angled photoetching technique for dry adhesion, which is considered as a key technique for switching the adhesive force over the solid–solid interface. Upon a rotating magnetism-stimuli, the tilted microcilia/pillars could be harnessed for the droplets controllable tranport.[15–19] More recently, by taking advantage of loading external pressure with the assistance of heating, the slanted shape memory polymer (SMP) pillar-arrays could be obtained for the fluids rectification.[20–24] These previously reported studies provide profound experimental and theoretical guidance for artificially building the slanted species. However, several apparent shortages subsequently raised: (1) Typical manufacturing strategies for slanted structures (e.g., lithography, DRIE, and VPP) suffer from the sophisticated operation and time-consuming process, which greatly hinders their practical usage. (2) To date, achieving the functionalities of droplet controllable migration and dry adhesion on the same slanted pillar-arrayed surface has been rarely examined. As a result, developing a more facile and effective route to fabricate a slanted microstructure with dual-functionalities (droplet maneuvering and dry adhesion) is still challenging and highly desirable.

To solve the above challenges, a thermal-responsive slanted shape memory microcone array (SSMMA) is facilely prepared by combining the femtosecond laser oblique microfabrication and replica-molding methods. The proposed SSMMA has a tilted angle of ∼45° (original state) and can achieve a large bending angle (>45°, collapsed state) in response to external stimuli (heating and pressing). The collapsed SSMMA restores to its original state within ∼10 s after being reheated above the glass transition temperature (T_g) of SMP, which attributes to its fast temperature-responsive feature. Furthermore, the influence of microcones spacing and morphological state of SSMMA on the wetting performance as well as the droplets adhesive dynamics are systematically investigated. The results indicate that the wettability and adhesion can be reversibly switched as the microcone array modulates between the collapsed and slanted states.[21,25,26] On this basis, the controllable droplet migration can be realized. More importantly, the SSMMA with a specific adhesion (maximum value ∼ 19.404 mN) can be used as a machine hand to transfer the smooth and fragile solid objects from the donor to the target substrate. These achievements are envisioned to extend the applications of SMP microstructures in the fields, such as directional liquid transportation, tunable wettability, and dry adhesion.

The SSMMA was fabricated using a combination of femtosecond laser oblique microfabrication and replica molding method as shown schematically in Figs. 1(a)–1(d). First, the silica gel membrane was

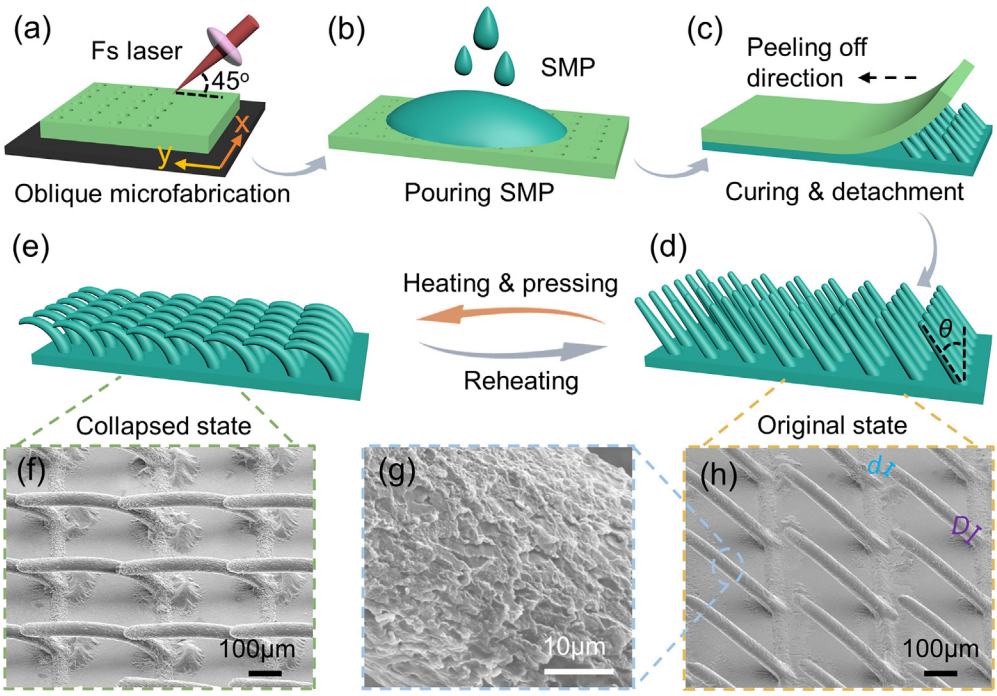

FIG. 1. (a)–(c) Schematic diagram of the fabrication process of SSMMA. (d) and (e) Schematic diagram of the reversible morphology conversion between the slanted state and collapsed state. (f) and (h) SEM images of microcone arrays in the collapsed and slanted states, respectively. (g) The magnified SEM image of microcone surface.

placed horizontally on a two-dimensional moving platform and then micro-drilled by a femtosecond laser with a tilted angle of 45° (Fig. S1). Subsequently, the SMP mixture was poured onto the silica gel template, which was modified with the release agent. The template was carefully peeled off along the tilted direction of the microcone after the SMP had been completely cured by storing in 60 °C for 2 h and then 100 °C for 1 h. The tidy SSMMA with a bending angle [θ, defined in Fig. 1(d)] of 45° could be harvested. Notably, the SMP composite was composed of diglycidyl ether of bisphenol A, n-octylamine, and m-xylylenediamine with the relative molar ratio of 4:2:1 (see the supplementary material for more details).[27] Due to its thermo-triggered shape memory effect, the SSMMA can be transformed into a collapsed state under the external stimuli (heating and pressing) as depicted in Fig. 1(e), where the collapsed state can be maintained for a long time since the external pressure load was removed after suffering a natural cooling to the room temperature (Fig. S2). After being reheated, it would recover to its original slanted state [Fig. 1(d)]. The structural integrity of the microcone arrays was further confirmed by the scanning electron microscopy (SEM) images as shown in Figs. 1(f) and 1(h). Giving a fitting analysis in Fig. S3, the distribution of diameters conforms to a normal distribution, indicating that current SSMMA has a good consistency of the microcone diameters. The bottom diameter (D) and top one (d) of the microcones were measured as 55 ± 1.7 and $30 \pm 1.4\,\mu$m, respectively. Moreover, the collapsed microcone array was still neat, which is the unique advantage of the slanted microcone array in comparison with the upright one. The magnified SEM image in Fig. 1(g) shows that the obtained microcone profile was covered with some rough structures, which originates from the topography of the inner surface of the silica gel template (Fig. S4).

Due to the flexibility of femtosecond laser processing, the microcone array with a spacing of 100, 300, and 500 μm could be obtained with ease. The SEM images and the inserted optical pictures in Fig. 2(a) evidence the uniformity of SSMMA from different perspectives. Other designed SSMMAs with pillar spaces of 200, 400, and 600 μm are shown in Fig. S5. Additionally, the SSMMAs with different heights (H, 120–500 μm) could be readily obtained by altering the pulse number of the laser, as shown in Fig. S6. Notably, the taper ratio varies from 1:5.3 to 1:16.7 as the H increases from 120 to 500 μm (Fig. S7 and Table S1). Subsequently, in Fig. 2(b), the thermomechanical property of the SMP composites was also investigated using the dynamic mechanical analysis (DMA) strategy. The storage modulus decreased from ~1.1 GPa at 20 °C to ~3.5 MPa at 100 °C. Accordingly, the peak temperature of the tan δ (loss tangent) curve reveals that the SMP's T_g is about 77 °C. That is, the SMP sample can become soft when the temperature exceeds T_g. The above experimental result grants researchers a guidance for selecting the desirable temperature for

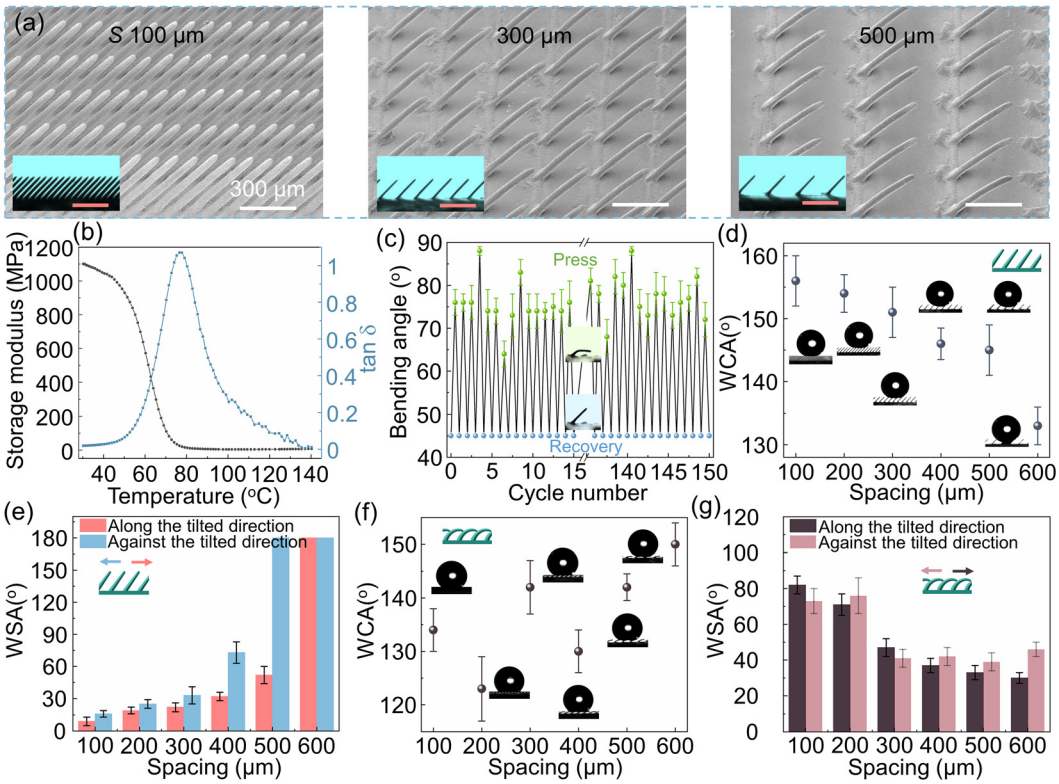

FIG. 2. (a) SEM images of SSMMAs with S is 100, 300, and 500 μm, respectively. The inset optical pictures are the side view of SSMMAs (scale bar: 600 μm). (b) The influence of temperature on the storage modulus and tan δ of the SMP sample. (c) The variation of bending angle of the microcone array after different cycles of pressing and recovery. (d) and (f) The contact angles of water droplets on the slanted and collapsed microcone arrays, respectively. (e) and (g) The sliding angles of water droplets on the slanted and collapsed microcone arrays, respectively.

maneuvering the pillar's state. Typically, in the current study, an actuating temperature of 120 °C was adopted for triggering the SMP sample. As shown in Figs. S8 and S9, the collapsed microcone array ($\theta \sim 83°$) could be restored to its original state ($\sim 45°$) within 10 s with a displacement rate of 32.56 μm/s after being heated at 120 °C on a mini hot plate. In contrast, θ of the original slanted microcone array remains unchanged even after being heated at 120 °C (Movie S1, the supplementary material). This phenomenon indicates that the collapsed microcone array can be quickly restored to its original state under a high temperature ($T > T_g$). The fatigue stability of the slanted microcone was also carried out by measuring the θ as long as 150 cycles of the alternately pressing/recovery process [Figs. 2(c) and S10]. The result unfolds that the current SSMMA has ultra-robust durability even though suffering from cyclic heating/cooling operations. The bending angle of the microcone remains to be located at $\sim 45°$ after each recovery process, indicating that the current SSMMA has good stability owing to the cross-linking network of SMP (Fig. S11).

To investigate the wettability of the obtained sample, the SSMMA with different S (100 to 600 μm) and the same H (500 μm) were prepared. As shown in Fig. 2(d), the water contact angle (WCA) values on the SSMMA surface gradually decreased from 156° to 133° as S increased from 100 to 600 μm. As can be seen from the optical images, the droplets gradually penetrated into the gaseous gap among the microcones with the increase in S, which is well consistent with the result of a previous study.[28] As S increases to a certain level (e.g., 600 μm), the contact state of the droplet changed from the "Cassie–Baxter state" to the "Wenzel state." Although the variation of WCA is limited, the variation of water sliding angle (WSA) is obvious. Figure 2(e) evidences that the WSA is closely correlated with S. That is, with the increase in S, the droplet's sliding behavior changed from easy-sliding with a small tilting angle to a pinning state. Notably, the WSA against the tilted direction was always larger than that along the tilted direction, apart from a specific sample with the S of 600 μm. It should be noted that the anisotropy for the sample with a spacing of 500 μm is the most evident one.

We also evaluated the wettability of the collapsed microcone array as θ changed to $\sim 80°$ after being pressed. Figure 2(f) shows that the collapsed microcone array also unfolded the hydrophobicity ($120° < \mathrm{WCA} < 150°$). The air layer captured in the microstructure becomes apparent as S increases from 100 to 600 μm. Additionally, as depicted in Fig. 2(g), the WSAs of the collapsed microcone arrays with the S of 100 and 200 μm are higher than those with larger spacing arrays (300, 400, and 500 μm). The difference in WSA between two different sliding directions is small for all the collapsed microcone arrays, which should be attributed to a much more flat surface assigned to the collapsed microcone array leading to the reduction in the anisotropy.

In addition, the relationship of WCA with θ was also studied. As seen from Fig. S12, the WCA decay from $\sim 154°$ to $\sim 148°$ as the θ elevated from 45° to 80°, indicating that θ has a limited effect on the wettability of SSMMA.

To gain a better understanding of the above-mentioned phenomenon, we established the theoretical model as shown in Fig. 3. If S is sufficiently small (e.g., 100 μm), the contact mode between the droplet and the microcones is Cassie–Baxter state. In this case, the contact area is small and the triple-phase contact line [TCL, red solid lines depicted in Fig. 3(a)] is short. As S increased, the droplets penetrated into the gaseous gap among the micropillars. If S is large enough (e.g., 600 μm), the droplets are immersed completely into the microstructures, which is a Wenzel state. At this stage, the contact area was enlarged compared to the initial contact area, resulting in a longer TCL (red dashed line) as displayed in Fig. 3(b).

Noting that the adhesive force (F_a) between the microcones and the droplet is very different for the above two separate contact states. F_a can be evaluated by the following equation:[19]

$$F_a = \gamma \times L,$$

where the γ and L represent the surface tension of the droplet and the length of TCL, respectively.

It can be concluded from the above equation that F_a generated by the microcone array with a denser S (lower adhesion, F_{a1}) is far smaller than that generated by the microcone array with looser S (high adhesion, F_{a2}), owing to the different length of TCL.[29] As such, the SA of the droplet on the former is much smaller than that on the latter. In addition, the SA along the tilted direction is not distinctly different from the one against the tilted direction for microcone array with a smaller space, that is, the anisotropy is not apparent. In contrast, the anisotropy of the microcone array with a larger S (e.g., 500 μm) is more obvious.

The variation of surface wettability on the SSMMA with different S has been explicitly discussed. Next, we further clarify the mechanism for the change of surface wettability on the collapsed microcone arrays. The schematics in Figs. 3(c) and 3(d) show the wetting state of droplets on the collapsed microcone arrays, indicating that the collapsed microcone array still exhibited the hydrophobicity with the increase in S. The top-view SEM images in Figs. 3(e) and 3(f) show that the larger and smaller spacing microcone arrays have different morphologies after being collapsed. The smaller spacing microcone arrays formed a disorganized and overlapped structure after being collapsed, while the larger spacing ones formed a "head to tail" structure. The top-view images in Figs. 3(e1) and 3(f1) show that the denser spacing microcone array has a larger contact area with regard to the droplet comparing with that of the looser spacing one. A larger contact area contributed to a longer TCL. Thus, the adhesion force on the smaller spacing microcone arrayed surface (e.g., 100 μm) is greater than that on the larger spacing microcone arrayed one (e.g., 600 μm).

Subsequently, the dependence of droplet's adhesion force on H was further explored. The slanted microcone arrays with different H exhibit excellent superhydrophobic properties [$\mathrm{WCA} > 150°$, Fig. S13(a)]. As H increased from 120 μm to 500 μm, the sliding angles of the droplet along/against the tilted direction were always maintained at $\sim 21°/31°$ [Fig. S13(b)], indicating that the change in H has an inferior influence on the droplet's adhesion. In contrast, the collapsed microcone array still remained the hydrophobic properties [$140° < \mathrm{WCA} < 150°$, Fig. S13(c)], and the sliding angle did not have an apparent change [Fig. S13(d)]. Signifying that regulating H could not contribute to a considerable change in terms of the adhesion force over the collapsed microcone-arrayed surface.

In addition, the adhesion force of the droplet movement in the anti-tilted direction of collapsed and original SSMMA ($S \sim 500$ μm) was also performed by using a customized surface force apparatus (Fig. S14). As can be seen from Fig. 4(a), the adhesion force of the

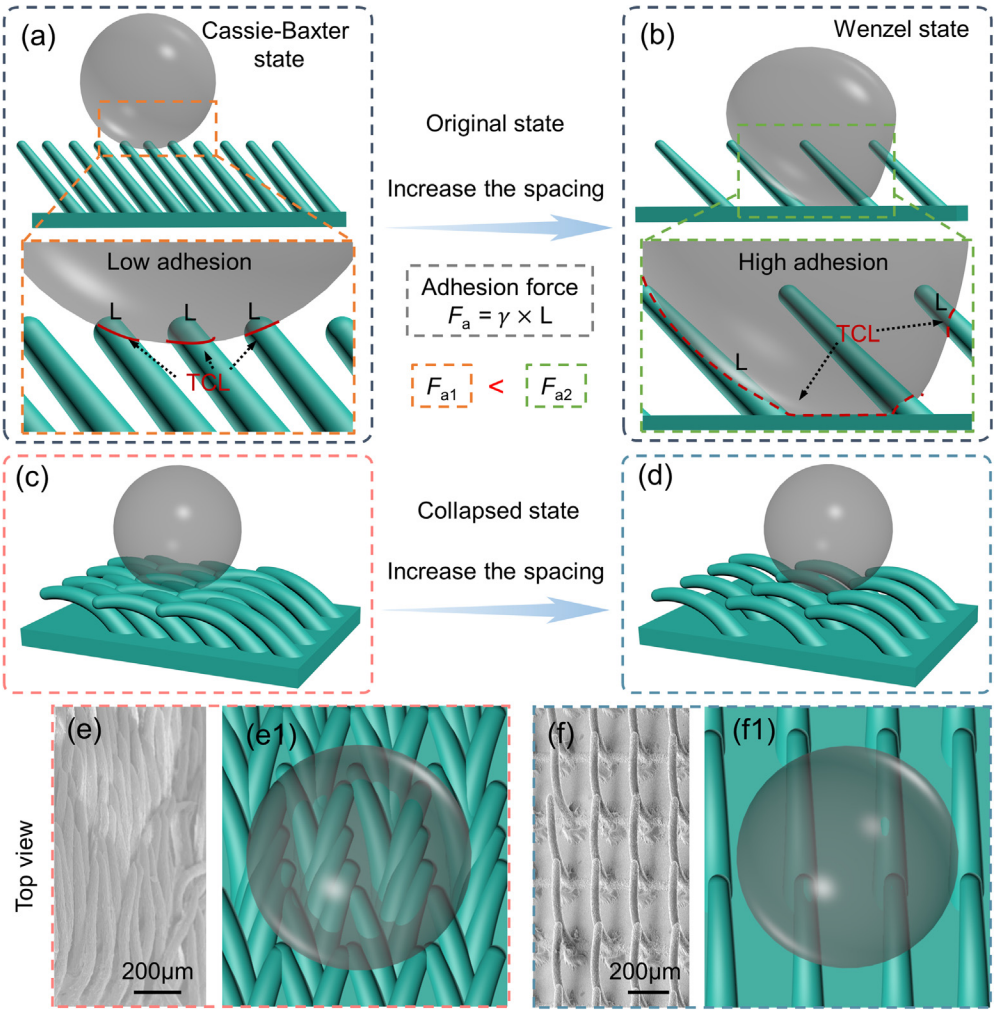

FIG. 3. (a) and (b) Schematic diagram of the change in droplet contact state on the tilted microcone array as the spacing increases. (c) and (d) Schematic diagram of the change in droplet contact state on the collapsed microcone array as the spacing increases. (e) and (f) The top-view SEM images of the collapsed microcone arrays with big and small spacing. (e1) and (f1) Top-viewed schematic diagram of the droplet contact state on the collapsed microcone array with big and small spacing.

droplet on the collapsed microcone array was measured as ∼60 μN, which was much smaller than the measured figure ∼104 μN on the original SSMMA. The result is very consistent with the sliding behaviors that are presented in Figs. 2(e) and 2(g). On these bases, we designed a droplet manipulation platform to achieve the controllable droplet transport by tuning the morphology of the microcone array with the S of 500 μm. First, the collapsed microcone array was attached to the mini-hot plate as shown in Fig. 4(b). Then, it was anchored with a tilted angle (α) of 50° (Fig. S15). Finally, the morphology transformation of the microcone array could be realized by controlling the switch of a hot plate. To thoroughly understand the mechanism of switching the droplet between sliding and pining, the force analysis was studied in detail. As depicted in Fig. 4(b), three main forces acted on the droplet as it slides on the collapsed microcone array: the gravity G, the support force F_s, and the adhesion force F_a. F_s is equal to the vertical-direction component of the gravity ($G \cos \alpha$), so they equilibrated each other and could be, therefore, neglected. Therefore, the driving force (F_d) of the droplet is derived from the axis-direction component of G, i.e., $F_d = G \sin \alpha$. As discussed in Fig. 3(f1), the droplet was supposed to have a smaller $F_{a'}$ on the collapsed microcone array with a larger S. In this case, F_d is sufficient to overcome $F_{a'}$, resulting in a resultant force downward along the tilted surface. Eventually, the droplet could slide down from the surface [Fig. 4(d) and Movie S2, the supplementary material], indicating that the collapsed microcone arrays were more beneficial for the droplets transport. Partial collapsed microcone array returned to its original slanted state (45°) when the mini-hot plate was switched on [Fig. 4(c)]. When the droplet slid from the collapsed microcone array to the slanted microcone array, the droplet fallen into the gaseous gap among the slanted microcones and finally dwelt on the surface [Fig. 3(c)]. As shown in Fig. 4(e), the droplet pinned onto the SSMMA because the component force of gravity (F_d) fails to overcome the adhesion force $F_{a''}$. This phenomenon indicates

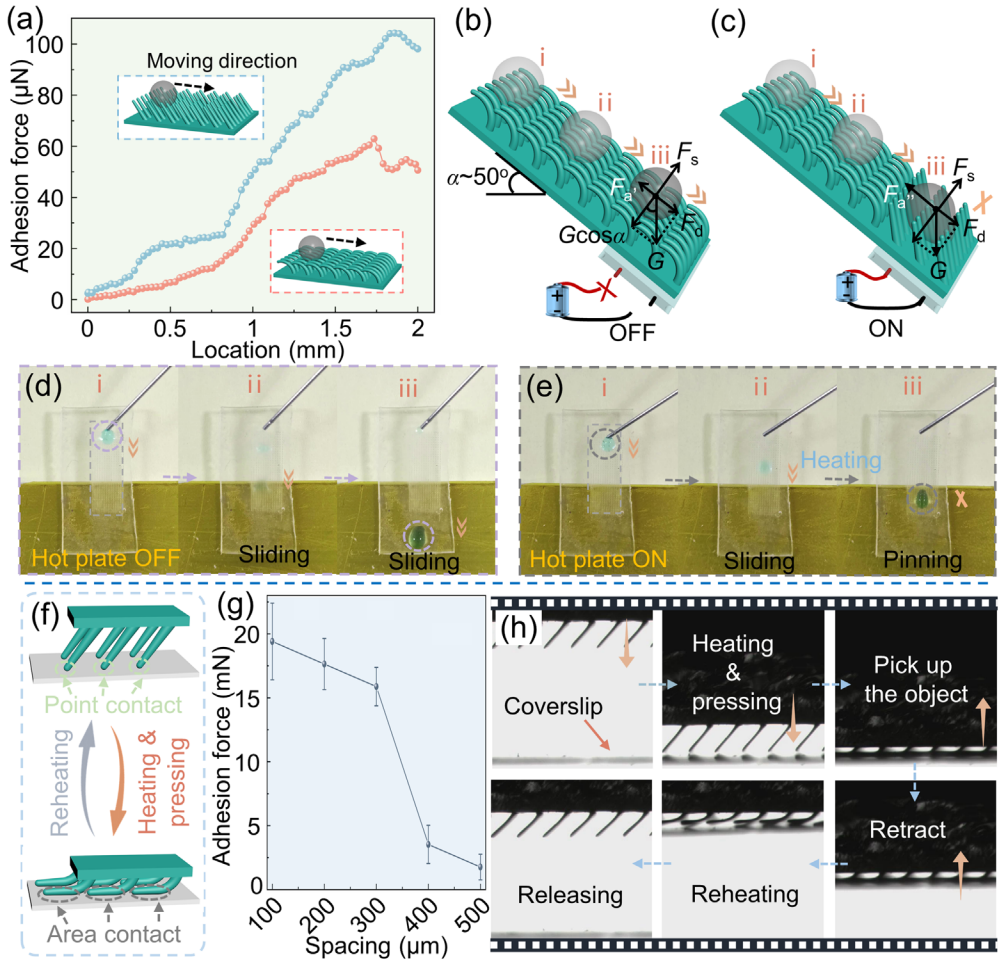

FIG. 4. (a) Adhesion force of droplet on the collapsed and slanted microcone arrays ($S \sim 500\ \mu m$) during moving against the tilted direction. (b) and (d) The schematic diagram and photographs of water droplets sliding on the collapsed microcone array. (c) and (e) The schematic diagram and photographs of the droplet sliding behavior interrupted by a heated restored microcone array. (f) Schematic diagram illustrating the process of dry adhesion. (g) The adhesion force of microcone array with different spacings. (h) The capture and release process of coverslip by microcone array.

that our structure can achieve the switch of droplet between sliding and pinning dynamics, which provides an efficient way for droplet manipulation.

Similarly, inspired by the gecko foot hairs,[30,31] current SSMMA with tunable adhesion as a dry adhesive to manipulate the fragile object is also demonstrated. As a proof-of-concept, we selected a smooth coverslip (~0.18 g, $20 \times 20 \times 0.15\ mm^3$) with the roughness of 236 nm as the manipulated object (Fig. S16). Initially, the tips of the rigid SSMMA were carefully controlled to contact with the coverslip (point contact) as shown in Fig. 4(f). After being heated above its T_g, it will become a compliant rubbery state.[32] A flat region between the microcone arrays and the object could be formed under a certain load. We defined this contact state as "area contact," that is, a large adhesion force is formed between the collapsed microcone array and the object. The microcone arrays would maintain the collapsed state (area contact) after cooling down below T_g and restored to its original shape (point contact) after being reheated. Therefore, the controllable surface adhesion was achieved arising from the switchable contact state, which unfolds a significant potential in dry adhesion. Subsequently, the adhesion force of microcone arrays ($\sim 5 \times 5\ mm^2$) with different S (100–500 μm) at the same θ (~80°) and H (~500 μm) was investigated [Fig. 4(g)]. The specific test process is shown in Fig. S17 and detailedly introduced in our experimental section (the supplementary material). It can be found that the adhesion force decreased from 19.404 to 1.764 mN as the S increased from 100 to 500 μm, implying that the microcone array with a smaller S should have a more robust adhesion force. Typically, we attempted to achieve the coverslip transfer by the as-prepared SSMMA with the S of 300 and H of 500 μm. As seen from Fig. 4(h) and Movie S3 (the supplementary material), the coverslip could be easily transferred to the target location without any damage. This work evidenced that the scot-free transfer of smooth fragile object could also be achieved by SSMMA. Additionally, in comparison with the previously explored platforms for dry adhesion,[33–36] which unfolds either a complicated fabricating process or a single

function, the current SSMMA is superior to their microstructures with regard to a more facile molding (one-step femtosecond laser oblique microfabrication) and a bi-functional merit (dry adhesion and drops steering) (Fig. S18). Therein, we also execute the comparison of the dry adhesion force per unit area between current SSMMA and other platforms, that is indeed a pressure (P). Current thermo/stress-responsive SSMMA is demonstrated to have a relative moderate P of 0.8×10^3 Pa, which could not reach the magnitude as other platforms $\sim 10^6$ Pa. Considering that dry adhesion is not only related to the morphology of micro-/nano-structures, but the dragging speed and other factors also affect the resulted P. In this study, by proposing a bifunctional SSMMA, we mainly focus the surface wettability switching, that is, the dry adhesion force maneuvering is dramatically harvested as a by-product.

In summary, a bi-functional SSMMA was proposed by combining the femtosecond laser oblique microfabrication and replica-mold method for maneuvering the droplet behavior and dry adhesion. Due to its shape memory effect and temperature-responsive merits, the wettability and adhesion force of water droplets can be adjusted by manipulating the SSMMA's morphology switching between the slanted state and the collapsed one. On this basis, the migration behavior of surface droplets can be tuned between sliding and pinning with ease in response to alternate adhesive forces. In addition, the collapsed SSMMA could be adhered to a smooth object by an adhesion force $\sim$19.404 mN, which has been employed as a machine hand to achieve the dynamic transfer of fragile devices with no damage. This work will not only aid the development of microfluid manipulation technology but also boost available avenues for dry adhesion transfer of fragile devices.

See the supplementary material for the experimental section, the thermal response effect of shape memory microcones, control the sliding behavior of droplets on microcone surface, adhesion and release of smooth and fragile object using microcone array.

This work was supported by the National Natural Science Foundation of China (Grant Nos. 51875160, 52005475, and 51805508), the Fundamental Research Funds for the Central Universities (Grant Nos. PA2020GDKC0010, PA2020GDSK0077, and JZ2021HGTB0101), the Hefei Natural Science Foundation (No. 2021020), the Qing Lan Project of the Jiangsu Province Higher Education Institutions of China (2019), the Basic Science Research project of Nantong municipality (No. JC2020079), the Natural Science Foundation of Jiangsu Province (Grant No. BK20191209), and the Excellent Scientific and Technological Innovation team project of Jiangsu Province (Grant No. 2021-52). The authors acknowledge the Experimental Center of Engineering and Material Sciences at USTC and the Intelligent Interconnected Systems Laboratory of Anhui Province at HFUT for the fabrication and measuring of samples.

AUTHOR DECLARATIONS

Conflict of Interest

The authors declare no conflicts of interest.

DATA AVAILABILITY

The data that support the findings of this study are available from the corresponding authors upon reasonable request.

REFERENCES

[1]H. Lu, B. Wu, X. Yang, J. Zhang, Y. Jian, H. Yan, D. Zhang, Q. Xue, and T. Chen, "Actuating supramolecular shape memorized hydrogel toward programmable shape deformation," Small **16**, 2005461 (2020).
[2]T. Wong, S. Kang, S. Tang, E. Smythe, B. Hatton, A. Grinthal, and J. Aizenberg, "Bioinspired self-repairing slippery surfaces with pressure-stable omniphobicity," Nature **477**, 443–447 (2011).
[3]M. Hancock, K. Sekeroglu, and M. Demirel, "Bioinspired directional surfaces for adhesion, wetting, and transport," Adv. Funct. Mater. **22**, 2223–2234 (2012).
[4]X. Gao and L. Jiang, "Water-repellent legs of water striders," Nature **432**, 36 (2004).
[5]L. Xiao, G. Li, Y. Cai, Z. Cui, J. Fang, H. Cheng, Y. Zhang, T. Duan, H. Zang, S. Li, Z. Ni, and Y. Hu, "Programmable 3D printed wheat awn-like system for high-performance fogdrop collection," Chem. Eng. J. **399**, 125139 (2020).
[6]A. Börner, M. Schäfer, A. Schmidt, M. Grau, and J. Vorwald, "Associations between geographical origin and morphological characters in bread wheat (*Triticum aestivum* L.)," Plant Genet. Resour. **3**(3), 360–372 (2005).
[7]R. Elbaum, L. Zaltzman, I. Burgert, and P. Fratzl, "The role of wheat awns in the seed dispersal unit," Science **316**, 884–886 (2007).
[8]Y. Su, L. Chen, Y. Jiao, J. Zhang, C. Li, Y. Zhang, and Y. Zhang, "Hierarchical hydrophilic/hydrophobic/bumpy Janus membrane fabricated by femtosecond laser ablation for highly efficient fog harvesting," ACS Appl. Mater. Interfaces **13**, 26542–26550 (2021).
[9]S. Yi, J. Wang, Z. Chen, B. Liu, L. Ren, L. Liang, and L. Jiang, "Cactus-inspired conical spines with oriented microbarbs for efficient fog harvesting," Adv. Mater. Technol. **4**, 1900727 (2019).
[10]H. Zhou, M. Zhang, C. Li, C. Gao, and Y. Zheng, "Excellent fog-droplets collector via integrative Janus membrane and conical spine with micro/nano-structures," Small **14**, 1801335 (2018).
[11]K. Chu, R. Xiao, and E. Wang, "Uni-directional liquid spreading on asymmetric nanostructured surfaces," Nat. Mater. **9**, 413–417 (2010).
[12]N. Malvadkar, M. Hancock, K. Sekeroglu, W. Dressick, and M. Demirel, "An engineered anisotropic nanofilm with unidirectional wetting properties," Nat. Mater. **9**, 1023–1028 (2010).
[13]Z. Wang, "Slanted functional gradient micropillars for optimal bioinspired dry adhesion," ACS Nano **12**, 1273–1284 (2018).
[14]H. Jeong, J. Lee, H. Kim, S. Moon, and K. Suh, "A nontransferring dry adhesive with hierarchical polymer nanohairs," Proc. Natl. Acad. Sci. U. S. A. **106**, 5639–5644 (2009).
[15]M. Cao, X. Jin, Y. Peng, C. Yu, K. Li, K. Liu, and L. Jiang, "Unidirectional wetting properties on multi-bioinspired magnetocontrollable slippery microcilia," Adv. Mater. **29**, 1606869 (2017).
[16]H. Wang, Z. Zhang, Z. Wang, Y. Liang, Z. Cui, J. Zhao, X. Li, and L. Ren, "Multistimuli-responsive microstructured superamphiphobic surfaces with large-range, reversible switchable wettability for oil," ACS Appl. Mater. Interfaces **11**, 28478–28486 (2019).
[17]Y. Lin, Z. Hu, M. Zhang, T. Xu, S. Feng, L. Jiang, and Y. Zheng, "Magnetically induced low adhesive direction of nano/micropillar arrays for microdroplet transport," Adv. Funct. Mater. **28**, 1800163 (2018).
[18]Y. Peng, Y. He, S. Yang, S. Ben, M. Cao, K. Li, K. Liu, and L. Jiang, "Magnetically induced fog harvesting via flexible conical arrays," Adv. Funct. Mater. **25**, 5967–5971 (2015).
[19]Y. Song, S. Jiang, G. Li, Y. Zhang, H. Wu, C. Xue, H. You, D. Zhang, Y. Cai, J. Zhu, W. Zhu, J. Li, Y. Hu, D. Wu, and J. Chu, "Cross-species bio-inspired anisotropic surface for active droplets transportation driven by unidirectional microcolumn waves," ACS Appl. Mater. Interfaces **12**(37), 42264–42273 (2020).
[20]Y. Jiao, C. Li, S. Wu, Y. Hu, J. Li, L. Yang, D. Wu, and J. Chu, "Switchable underwater bubble wettability on laser-induced titanium multiscale micro-/nanostructures by vertically crossed scanning," ACS Appl. Mater. Interfaces **10**, 16867–16873 (2018).
[21]J. Huo, X. Bai, J. Yong, Y. Fang, Q. Yang, X. Hou, and F. Chen, "How to adjust bubble's adhesion on solid in aqueous media: Femtosecond laser-ablated patterned shape-memory polymer surfaces to achieve bubble multi-manipulation," Chem. Eng. J. **414**, 128694 (2021).

[22]Y. Zhang, Y. Li, Y. Hu, X. Zhu, Y. Huang, Z. Zhang, S. Rao, Z. Hu, W. Qiu, Y. Wang, G. Li, L. Yang, J. Li, D. Wu, W. Huang, C. Qiu, and J. Chu, "Localized self-growth of reconfigurable architectures induced by a femtosecond laser on a shape-memory polymer," Adv. Mater. **30**, 1803072 (2018).
[23]H. Zhang, H. Lai, Z. Cheng, D. Zhang, P. Liu, Y. Li, and Y. Liu, "In-situ switchable superhydrophobic shape memory microstructure patterns with reversible wettability and adhesion," Appl. Surf. Sci. **525**, 146525 (2020).
[24]X. Bai, Q. Yang, Y. Fang, J. Zhang, J. Yong, X. Hou, and F. Chen, "Superhydrophobicity-memory surfaces prepared by a femtosecond laser," Chem. Eng. J. **383**, 123143 (2020).
[25]Z. Cheng, D. Zhang, T. Lv, H. Lai, E. Zhang, H. Kang, Y. Wang, P. Liu, Y. Liu, Y. Du, S. Dou, and L. Jiang, "Superhydrophobic shape memory polymer arrays with switchable isotropic/anisotropic wetting," Adv. Funct. Mater. **28**, 1705002 (2018).
[26]D. Zhang, Z. Cheng, and Y. Liu, "Smart wetting control on shape memory polymer surface," Chem. Eur. J. **25**, 3979–3992 (2019).
[27]Y. Jiao, C. Li, J. Ji, Z. Wang, T. Tao, T. Zhang, and K. Liu, "Femtosecond laser-induced shape memory polymer micropillar with tunable wettability and reversible adhesion for underwater oil droplet lossless transfer," Appl. Phys. Lett. **118**, 033701 (2021).
[28]C. Li, Y. Jiao, X. Lv, S. Wu, C. Chen, Y. Zhang, J. Li, Y. Hu, D. Wu, and J. Chu, "In situ reversible tuning from pinned to roll-down superhydrophobic states on a thermal-responsive shape memory polymer by a silver nanowire film," ACS Appl. Mater. Interfaces **12**, 13464–13472 (2020).
[29]C. Li, Y. Jiao, Y. Zhang, S. Jiang, X. Lv, S. Wu, J. Li, Y. Hu, J. Ye, K. Liu, D. Wu, and J. Chu, "Noncontact all-in-situ reversible reconfiguration of femtosecond laser-induced shape memory magnetic microcones for multifunctional liquid droplet manipulation and information encryption," Adv. Funct. Mater. **31**, 2100543 (2021).
[30]S. Kim and M. Sitti, "Biologically inspired polymer microfibers with spatulate tips as repeatable fibrillar adhesives," Appl. Phys. Lett. **89**, 261911 (2006).
[31]L. Boesel, C. Greiner, E. Arzt, and A. Campo, "Gecko-inspired surfaces: A path to strong and reversible dry adhesives," Adv. Mater. **22**, 2125–2137 (2010).
[32]J. Eisenhaure, T. Xie, S. Varghese, and S. Kim, "Microstructured shape memory polymer surfaces with reversible dry adhesion," ACS Appl. Mater. Interfaces **5**(16), 7714–7717 (2013).
[33]S. Kim, J. Wu, A. Carlson, S. Jin, A. Kovalsky, P. Glass, Z. Liu, N. Ahmed, S. Elgan, W. Chen, P. Ferreira, M. Sitti, Y. Huang, and J. Rogers, "Microstructured elastomeric surfaces with reversible adhesion and examples of their use in deterministic assembly by transfer printing," Proc. Natl. Acad. Sci. U. S. A. **107**(40), 17095–17100 (2010).
[34]Y. Mengüç, S. Yang, S. Kim, J. Rogers, and M. Sitti, "Gecko-inspired controllable adhesive structures applied to micromanipulation," Adv. Funct. Mater. **22**, 1246–1254 (2012).
[35]C. Linghu, S. Zhang, C. Wang, K. Yu, C. Li, Y. Zeng, H. Zhu, X. Jin, Z. You, and J. Song, "Universal SMP gripper with massive and selective capabilities for multiscaled, arbitrarily shaped objects," Sci. Adv. **6**, eaay5120 (2020).
[36]Y. Huang, N. Zheng, Z. Cheng, Y. Chen, B. Lu, T. Xie, and X. Feng, "Direct laser writing-based programmable transfer printing via bioinspired shape memory reversible adhesive," ACS Appl. Mater. Interfaces **8**, 35628–35633 (2016).